U.S. DEPARTMENT OF COMMERCE
National Oceanic and Atmospheric Administration
Environmental Research Laboratories

NOAA Technical Memorandum ERLTM-NSSL 52

THE EXPLORATION OF CERTAIN FEATURES OF TORNADO DYNAMICS USING A LABORATORY MODEL

Neil B. Ward

To Evelyn
from Neil

National Severe Storms Laboratory
Norman, Oklahoma
November 1970

TABLE OF CONTENTS

	Page
LIST OF FIGURES	v
ABSTRACT	1
1. INTRODUCTION	1
2. THE PHYSICAL MODEL	2
3. APPLICATION OF EULER'S MOMENTUM THEOREM	3
4. EXPERIMENTAL RESULTS	
4.1 Effect of the Configuration Ratio, $2r_o/h$, upon the θ, r_1 relationship.	8
4.2 Surface Pressure Profiles and the High Pressure Ring	10
4.3 The Vortex Core	13
4.4 Multiple Vortices	18
5. CONCLUSIONS	20
6. ACKNOWLEDGMENTS	21
7. REFERENCES	22

LIST OF FIGURES

Figure		Page
1	Vertical section of laboratory device.	2
2	Control volumes for application of momentum theorem.	4
3	Surface pressure profiles for various flows.	4
4	Variation of core diameter with inflow angle (Note inflow direction indicator lower right). (a) $\theta = 5°$, (b) $\theta = 12°$, (c) $\theta = 26°$, (d) $\theta = 32°$.	9
5	Core diameter vs inflow angle, $2r_o/h = 4$.	9
6	Core diameter vs inflow angle, $2r_o/h = 3$.	10
7	Core diameter vs inflow angle, $2r_o/h = 2.2$.	10
8	Surface pressure, $2r_o/h = 4$, no rotation.	11
9	Surface pressure, $2r_o/h = 4$, inflow angle $\theta = 6°$.	11
10	Surface pressure, $2r_o/h = 0.75$, inflow angle $\theta = 60°$.	11
11	Surface pressure comparison.	11
12	Surface pressure record for tornado cyclone of May 24, 1962.	12
13	Drawings of observed enlargement of vortex core, by Carl Reber.	14
14	Rotational stability in a column.	15
15	Laboratory vortex enlargement associated with transition from laminar to turbulent flow.	16
16	Flow schematic of vortex transition.	17
17	Tornado pair, Elkhart, Indiana, Palm Sunday, 1965.	17
18	Laboratory vortex pair.	18
19	Laboratory vortex family of three.	18
20	Observed surface flow for laboratory vortex pair.	19
21	Tornado path with suction spots (from Fujita, 1967).	20

THE EXPLORATION OF CERTAIN FEATURES OF TORNADO DYNAMICS USING A LABORATORY MODEL

Neil B. Ward

Three characteristic features of tornadoes are simulated in a laboratory system and the associated flow is observed and discussed. These are (1) a characteristic surface pressure profile, (2) a bulging deformation on the vortex core, and (3) multiple vortices in a single convergence system. Vortex motion is very sensitive to the geometrical features of the larger flow in which it is imbedded. Only when the diameter of the updraft column exceeds the depth of the inflow layer can features (1) and (3) be produced in the present model. When the updraft diameter is large compared to the depth of inflow, inertial effects associated with large changes in radial momentum produce significant convergent forces. When the updraft diameter is small compared to depth of inflow layer, the inflow speed is relatively small and related inertial effects are small. It is concluded that radial momentum flux is an important factor in the production of atmospheric vortices.

1. INTRODUCTION

The purpose of this study is to examine closely the role of the linear momentum possessed by the convergent layer of flow associated with tornado-producing thunderstorms. The study compares unique features of both tornadoes and laboratory produced vortices.

In vortex motion in the atmosphere, high rotational speeds near the center are associated with convergence and conservation of angular momentum. Even a very small tangential speed at a large radius in a fluid mass generates large rotational speeds near the center when convergence continues to a sufficiently small radius. Ignoring frictional losses, the angular speed is a function of radial position and for this reason, it appears that radial momentum needs to be given more consideration in vortex studies.

In atmospheric motion on the tornado scale, it is found that the area covered by the region of high rotational speed is generally very small compared to the area where strong convergence and vertical motion are taking place, and in tornado-producing thunderstorms, the convective area above the convergent flow field

may be an order of magnitude greater in diameter than the width of the tornadic windpath. More specifically, in the area of high tornado frequency in the United States, the converging layer that supplies the thunderstorm updraft may consist of a surface-based moist layer no more than one mile in depth while the diameter of the thunderstorm updraft is 5 miles or more. Therefore, one would expect to best simulate such convection by providing rising motion over an area appreciably greater in diameter than the depth of the converging layer. The ratio of the diameter to the depth is referred to here as the "configuration ratio."

The vortex features produced and observed in the laboratory have not been intricate. No attempt has been made to measure flow velocities or to find pressure distributions except over the lower surface of the flow cavity, and, as a result, the vortices produced have been undisturbed. Photography, both still and cinema, has been employed in conjunction with illumination of smoke tracers to record visually observed flow characteristics for subsequent study and analysis. Much of the observational material is unavoidably qualitative although quantitative determinations have been made of the inflow angles at the edge of the convection zone and of the core radii of the vortices. Measurement of the radial distribution of the static pressure at the lower surface has supplemented the observations of the fluid flow.

In the following sections of this discussion, line drawings are employed which often do not represent specific measurements but do portray, as truthfully as possible, visually observed and photographed flow patterns. Measurements are indicated in several instances as plotted points or are mentioned in the figure legends.

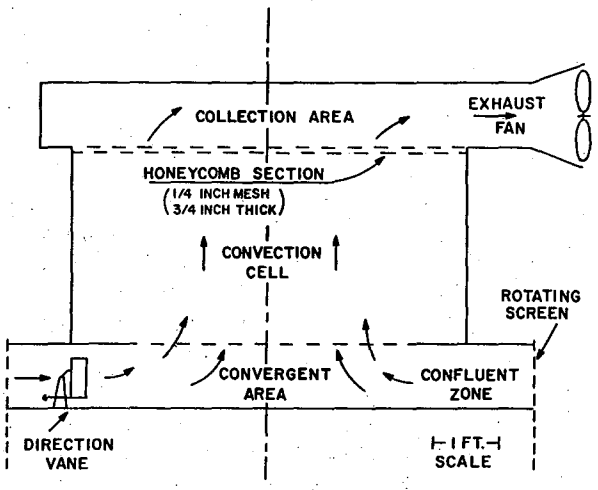

Figure 1. Vertical section of laboratory device.

2. THE PHYSICAL MODEL

Laboratory apparatus has been assembled to produce a flow system in which both the diameter of a rising air column and the depth of the inflow layer can be varied. The apparatus, figure 1, produces an adjustably convergent airflow through a fine mesh cylindrical wire screen, 8 feet in diameter, which imposes controlled angular momentum by its rotation around the perimeter. The convective flow is created by a variable speed exhaust fan with the pressure deficit

distributed over the top of the convective chamber, 6 feet in diameter and 3 feet high. At the top of the chamber, figure 1, the air passes through a relatively fine mesh honeycomb material which effectively removes the tangential component from the flow. This de-couples the vortex from the convection of the exhaust fan and roughly simulates conditions at the top of an atmospheric vortex.

When the convection diameter is large compared to the depth of inflow, a vortex core very small relative to the updraft diameter can be produced; the ratio may be of the order 1/50 or less. The inflow direction at the edge of the region of convection, under these conditions, is very nearly radial, the deviation being only 1 or 2 degrees. This means that the tangential component at the edge of the updraft is very small and is affected very little by frictional losses due to contact with the boundaries of the inflow zone. As a result, no secondary flows occur outside the core, such as the downward motion described by Ying and Chang (1970) and Kuo (1969).

The inflow angle, θ, relative to a radial, can be measured effectively by a small windvane in the confluent zone, figure 1, where the spiral angle is approximately constant. Pressure profiles along the lower surface are obtained by a static pressure port in the center of a flat sheet of metal moveable in an arc across the lower surface of the convergence area and connected through small tubing to an electronic manometer.

3. APPLICATION OF EULER'S MOMENTUM THEOREM

The interpretation of the observations of vortices produced with the laboratory system is facilitated through an application of the momentum theorem (Milne-Thomson, 1960) which pertains to fluid flow into and out of a volume, V, enclosed by a surface, S. The theorem states that

$$\int_S \vec{n} p \, dS = - \int_V \rho \vec{F} \, dV + \frac{\partial}{\partial t} \int_V \rho \vec{q} \, dV - \int_S n \cdot \vec{q} \rho \vec{q} \, dS \qquad (1)$$

where $\vec{n}$ is the inward unit vector normal to the surface, p is the static pressure*, ρ is the fluid density, $\vec{F}$ is the external force per unit mass, including gravity, t is time and $\vec{q}$ is the fluid velocity.

*Static pressure p as in the Bernoulli equation, $p + \rho g h + \rho V^2/2 =$ constant.

The flow is idealized to the extent indicated in figure 2, which shows the surface to which the theorem is applied, and by the following assumptions:

(1) the fluid density, ρ, is constant

(2) the flow is stationary so that $\frac{\partial}{\partial t}\int_V \rho\vec{q}dV$ is zero,

(3) external body forces and $\int_V \rho\vec{F}dV$ can be neglected,

(4) actual pressures at the surfaces (0) to (5) in figure 2 can be represented by average values which are cylindrically symmetrical,

(5) the inflow velocity at $r = r_o$ can be represented by an average, $\vec{q}_o$, having radial and tangential components whose magnitudes are u_o and v_o, respectively,

(6) angular momentum is conserved and

(7) friction is negligible.

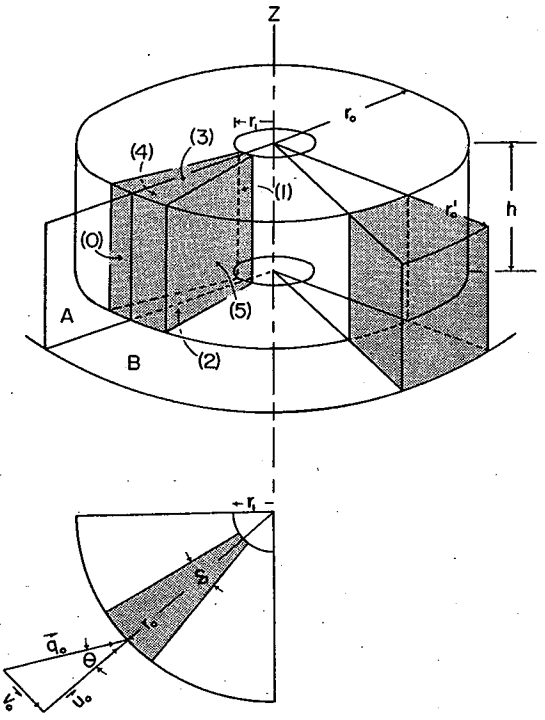

Figure 2. Control volumes for application of momentum theorem.

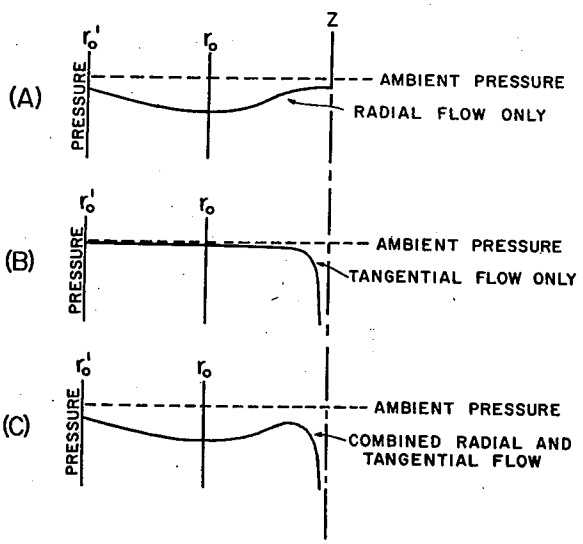

Figure 3. Surface pressure profiles for various flows.

The first three assumptions permit equation (1) to be shortened to

$$\int_S \bar{n} p dS = - \rho \int_S \bar{n} \cdot \bar{q}\bar{q} dS \qquad (2)$$

Returning to figure 2, h is the height of the inflow layer, r_o is the radius of the zone of convection and r_1 is the radius of the vortex core, both treated as vertical cylinders. Appropriate cylindrical coordinate reference planes, A and B, are, respectively, a vertical plane containing the Z-axis and bisecting the volume V and a horizontal plane coinciding with the lower boundary of the flow cavity. The Z-axis coincides with the central vertical axis of the vortex. The wedge angle, δ, is supposed to be small enough to allow the substitution of $\delta/2$ for sin $\delta/2$.

The vector equation (2) is equivalent to three scalar equations: one relating the radial pressure thrust and the efflux of radial momentum parallel to the A-plane, another relating the pressure thrust and the momentum efflux perpendicular to the A-plane and a third relating the pressure thrust and the momentum efflux perpendicular to the B-plane. These equations are:

$$\bar{p}_{4,5}(r_o - r_1)h\delta - (\bar{p}_o r_o - \bar{p}_1 r_1)h\delta = \rho u_o^2 r_o h\delta - \delta\rho \int_{r_1}^{r_o}\int_o^h v^2(r,z)drdz - \delta\rho \int_{r_1}^{r_o} w_3(r)u_3(r)rdr \qquad (3)$$

$$0 = -\rho u_o v_o r_o h\delta - \delta\rho \int_{r_1}^{r_o}\int_o^h v(r,z)u(r_1 z)drdz + \delta\rho \int_{r_1}^{r_o} w_3(r)v_3(r)rdr \qquad (4)$$

and

$$(\bar{p}_2 - \bar{p}_3)\delta(r_o^2 - r_1^2)/2 = \delta\rho \int_{r_1}^{r_o} w_3^2(r)rdr \qquad (5)$$

where the sign convention of a right-hand cylindrical coordinate system is employed and where:

$\overline{p_{4,5}}$ is the average pressure over a vertical radial section,

$\bar{p}_o$ and $\bar{p}_1$ are the average pressures on the cylindrical surfaces $r = r_o$ and $r = r_1$, respectively,

$\bar{p}_2$ and $\bar{p}_3$ are the average pressures on the lower and upper surfaces, respectively,

$u(r,z)$, $v(r,z)$ and $w(r,z)$ are the magnitudes of the components of the velocity $q(r,z)$ throughout the volume and

$u_3(r)$, $v_3(r)$ and $w_3(r)$ are the magnitudes of the components of the velocity $q_3(r)$ on the upper surface (3).

In the development of equations (3)-(5), it was assumed that the normal velocity component on the lower surface (2), where $z = 0$, and on the cylindrical surface (1), where $r = r_1$, is zero.

Equation (5) states that the efflux of momentum directed upward is equal to the net upward pressure thrust. Equation (4) is not of direct interest to this study, although it suggests an interpretation in terms of angular momentum flux. Equation (3), however, leads to a useful approximate relationship.

First, on the right side of (3), we interpret the initial term as a flow of radial momentum inward through side (0), the double integral as the centrifugal effect and the last integral as an unobserved small upward leakage of radial momentum through side (3). The double integral is simplified by applying the theorem of the mean to the inner integral,

$$\int_o^h v^2(r,z)dz = h\overline{v^2}(r), \tag{6}$$

and then approximating and using assumption (6), we write

$$h\overline{v^2}(r) \simeq v_o^2 r_o^2 h/r^2. \tag{7}$$

To this degree of approximation, the double integral becomes

$$v_o^2 r_o^2 \left(\frac{1}{r_1} - \frac{1}{r_o}\right)h \ .$$

Then, neglecting the leakage integral, dividing by $\rho v_o^2 r_o \delta h$, and rearranging terms on the right side, (3) becomes

$$\frac{(\bar{p}_{4,5} - \bar{p}_o)r_o - (\bar{p}_{4,5} - \bar{p}_1)r_1}{\rho v_o^2 r_o} = \frac{1}{\sin^2\theta} - \frac{r_o}{r_1} = K \qquad (8)$$

where θ, the inflow angle, is $\tan^{-1}\frac{v_o}{u_o}$.

Although (8) can be solved explicitly for r_1/r_o, it is more useful to rearrange and obtain

$$r_1 = r_o \frac{\sin^2\theta}{1 - K \sin^2\theta} \qquad (9)$$

where r_1, r_o and θ are observed flow parameters of the vortex in the physical model.

Radial pressure distributions relevant to this study are indicated by two special cases:

(1) When the inflow has no tangential component, v_o, $v(r,z)$ and r_1 become zero and (3) reduces to:

$$(\bar{p}_{4,5} - \bar{p}_o)r_o \delta h = \rho u_o^2 r_o \delta h \qquad (10)$$

where the leakage integral is again neglected. Since the right side of (10) is inherently positive, $\bar{p}_{4,5} > \bar{p}_o$, and the pressure distribution for values of $r < r_o$ must resemble that shown in figure 3(A).

(2) The second case relates to a truncated wedge of height h extending from surface (0) outward to a similar surface at a radius r_o' and lying within the inflow layer. Equation (3) now becomes

$$(\overline{p_{4,5}'} - \overline{p_o'})r_o' - (\overline{p_{4,5}'} - \overline{p}_o)r_o = \rho(u_o'^2 r_o' - u_o^2 r_o) \quad (11)$$

where $\overline{p}_{4,5}'$ and $\overline{p}_o'$ are, respectively, average pressures over a vertical section of the new volume V' and over the cylindrical surface $r = r_o'$, and u_o' is the radial velocity magnitude at $r = r_o'$. Noting that $u_o'r_o' = u_o r_o$ because of continuity and that $r_o' > r_o$ it follows that $p_o' > p_o$, indicating that the pressure in figure 3(A) increases outward toward ambient pressure p_a, in the region $r > r_o$.

Considering the conservative nature of the angular momentum in the converging fluid, the component of pressure due to tangential speed is

$$p_a - \frac{\rho}{2} \frac{v_o^2 r_o^2}{r^2} .$$

This component is shown in figure 3(B). Combining the pressure deficits indicated in 3(A) and 3(B) leads to figure 3(C), the expected resultant pressure profile due to radial flow with circulation.

4. EXPERIMENTAL RESULTS

4.1 Effect of the Configuration Ratio, $2r_o/h$, upon the θ, r_1 Relationship

Figure 4 shows how the value of r_1 and the associated inflow angle θ can be measured in the laboratory for comparison to (9). Smoke tracer introduced at the lower surface fills the turbulent, nondivergent core so that it can be measured by sighting across the vortex to a properly scaled rule.

Figure 5 shows a series of laboratory measurements made with the configuration ratio 4.0. These include a wide range of flow speeds and all show a reasonable correlation with (9) when K is equated to zero. While r_1 is very sensitive to changes in inflow angle, no correlation was found between r_1 and the total speed at the perimeter radius, r_o.

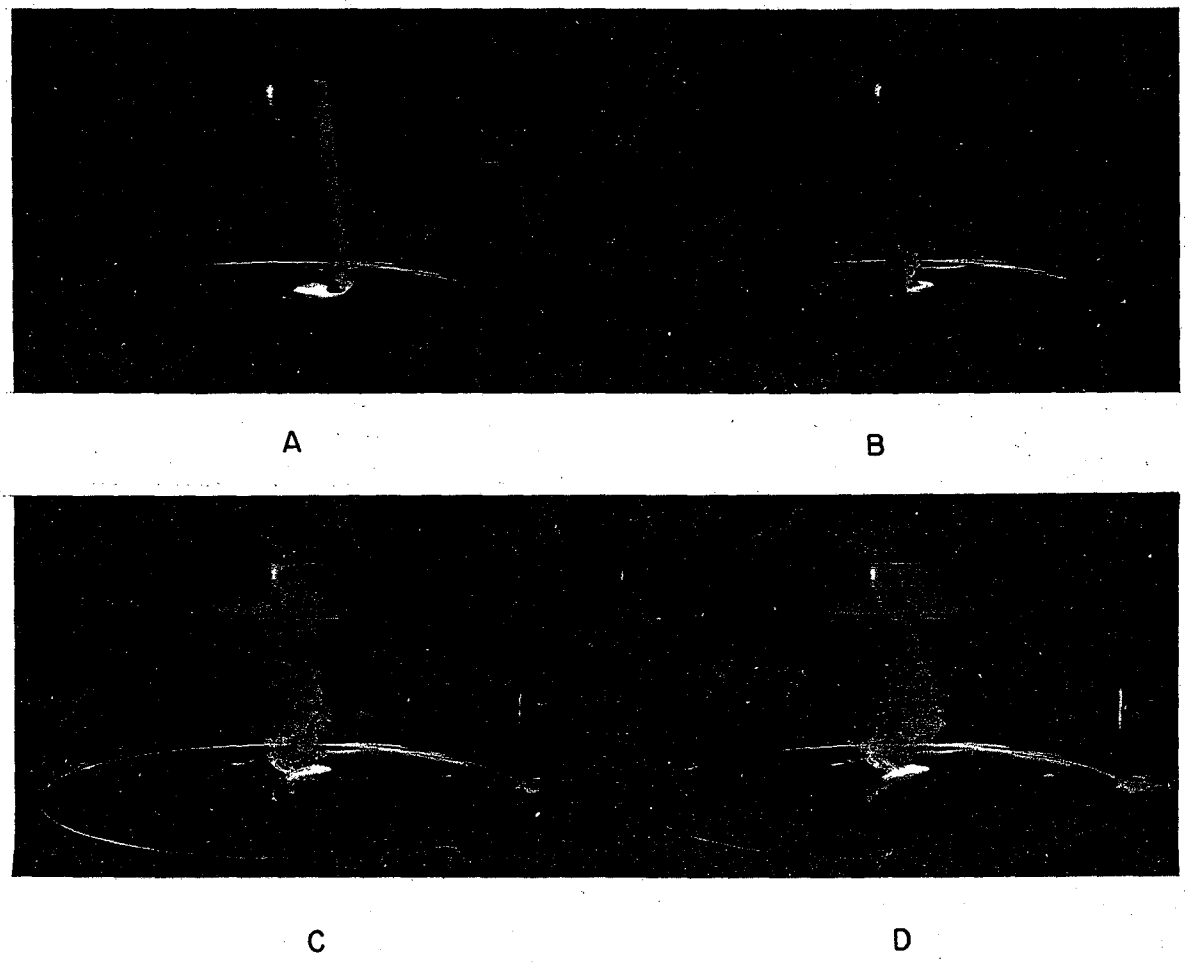

Figure 4. Variation of core diameter with inflow angle. (a) $\theta = 5°$, (b) $\theta = 12°$, (c) $\theta = 26°$, (d) $\theta = 32°$. (Above)

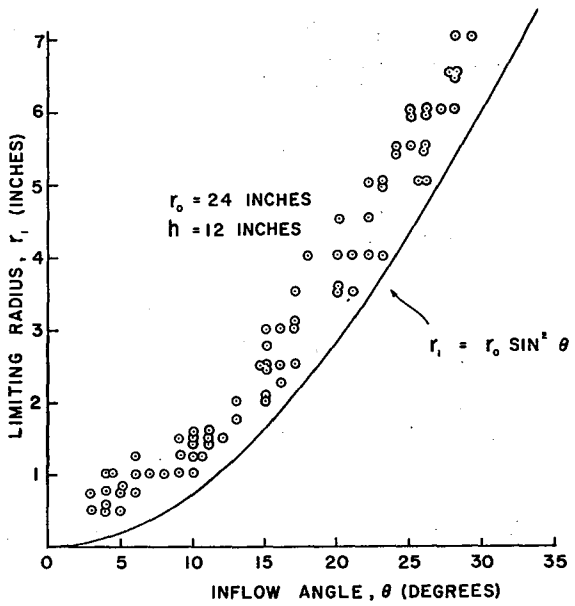

Figure 5. Core radius vs inflow angle, $2r_o/h = 4$. (Right)

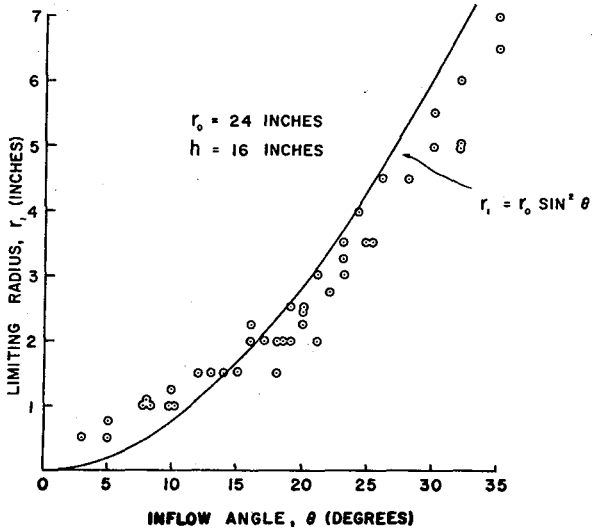

Figure 6. Core radius vs inflow angle, $2r_o/h = 3$.

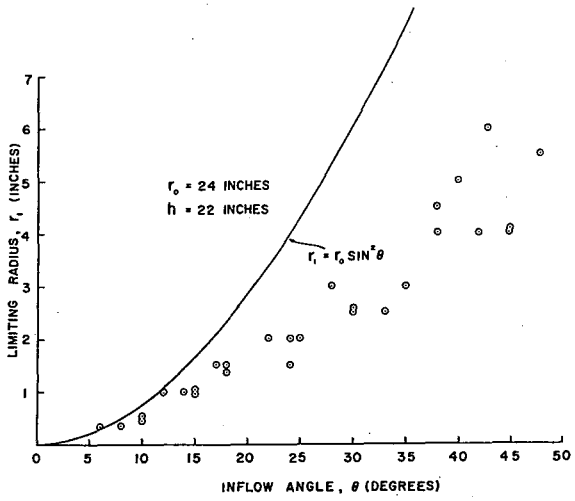

Figure 7. Core radius vs inflow angle, $2r_o/h = 2.2$.

If the configuration ratio is changed, the measured values of r_1 show an ordered deviation from (9). In figures 6 and 7 where $2r_o/h = 3.0$ and 2.2, respectively, it is seen that the radius of the vortex core becomes progressively smaller at the same inflow angle, indicating that K becomes increasingly negative as the ratio $2r_o/h$ decreases. This effect will be discussed more fully at the end of section 4.2 which deals with observed pressure distributions.

4.2 Surface Pressure Profiles and the High Pressure Ring

The surface pressure traces in figures 8-11 were obtained in the laboratory with the configuration ratio equal to 4.0 and 0.75. When the ratio is 4.0, the axial momentum flux at the top of the convergent layer approximates the radial momentum flux at the perimeter of the convection zone, while the smaller ratio requires the generation of momentum, since the average axial speed at the top of the convergent layer is over 5 times the average inflow speed at the convection perimeter.

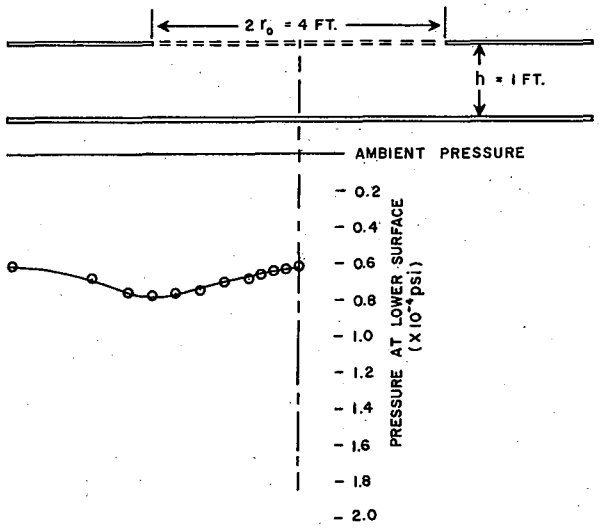

Figure 8. Surface pressure, $2r_o/h = 4$, no rotation.

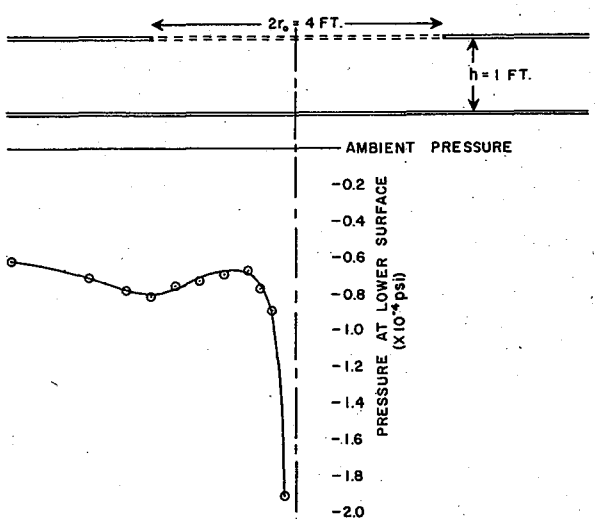

Figure 9. Surface pressure, $2r_o/h = 4$, inflow angle $\theta = 6°$.

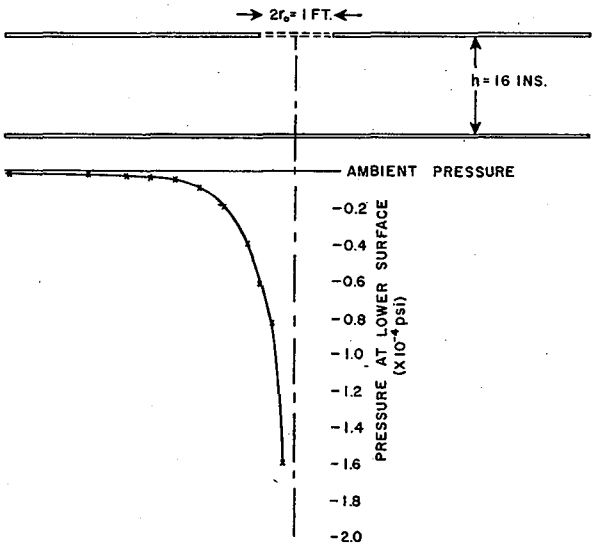

Figure 10. Surface pressure, $2r_o/h = 0.75$, inflow angle $\theta = 60°$.

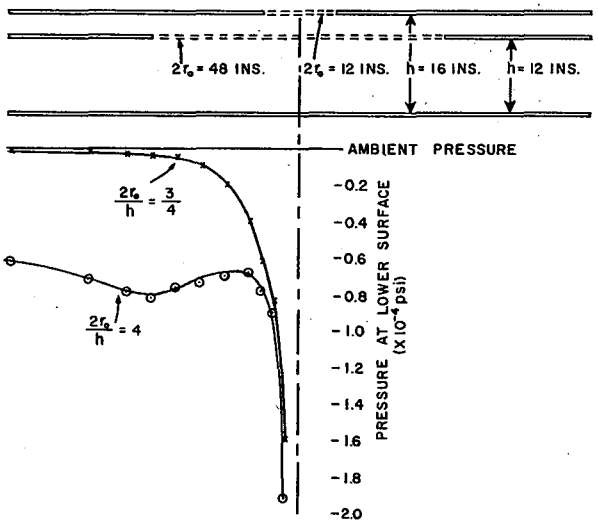

Figure 11. Surface pressure comparison.

Figure 8, where $2r_o/h = 4$, results with radial inflow only, when a minimum pressure at the updraft perimeter is associated with a maximum of radial inflow speed and a zero pressure gradient. As the flow approaches the center, the pressure increases as the radial speed decreases, reaching stagnation at the center. The area of high surface pressure is associated with vertical acceleration accompanying the convergence and matches qualitatively the distribution shown in figure 3(A), indicated by the momentum theorem.

In figure 9, the radial component of inflow at r_o and the configuration ratio are the same as in figure 8, but a small tangential component, about 1/10 the radial speed, has been added to the flow so that the inflow angle θ is now 6°. As the flow enters the zone of convection, there is very little difference in the outer portion of the pressure profiles, where the radial speed begins to decrease. As the air gets closer to the center, the tangential speed increases rapidly and the pressure decreases in a fashion resembling the pressure reduction in a free vortex as portrayed in figure 3(B).

Surface pressure profiles have been obtained from barographs as tornadoes passed overhead or nearby. They have frequently shown a well defined ring of relatively high surface pressure surrounding the vortex core and resembling that of figure 9 for the laboratory vortex when the configuration ratio is 4. Figure 12 is a copy of the barograph trace obtained when a tornado cyclone passed over a National Severe Storms Project barograph at Newton, Kansas, on May 24, 1962, (Ward, 1964).

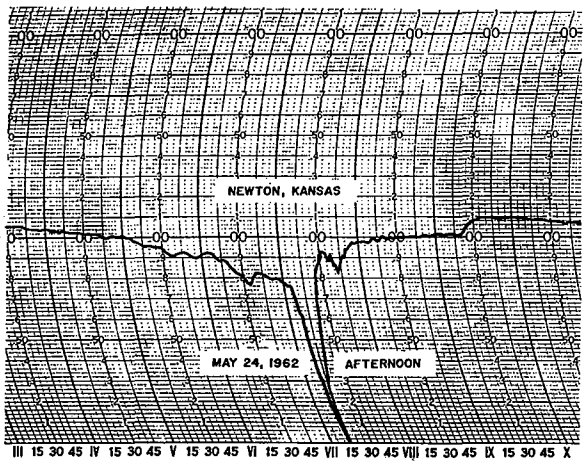

Figure 12. Surface pressure record for tornado cyclone of May 24, 1962.

Figure 10 shows a pressure profile observed when a vortex is formed with tangential speed about the same as in figure 9, but with the configuration ratio reduced to 0.75. Continuity requires a lower inflow speed to avoid excessive vertical velocity, and the inflow angle must be large for vortex formation. The profile in figure 10 was obtained with an inflow angle of 60°. In this example the minimum inflow angle for a detectable vortex core was about 30°, even though the applied pressure deficit was somewhat greater than in the example of figure 9. Note that at the perimeter of the

convection zone the pressure gradient force inward is large.

In figure 11, the surface pressure profiles for the two convective patterns are compared. In changing from the small configuration ratio to the large, it is apparent that, for the same vertical velocity, the radial inflow component at radius r = 24 inches must increase by a factor of about 21 to satisfy continuity. The increase in inflow speed is associated with a pressure decrease at that radius as indicated in the pressure profiles.

Returning for a moment to a consideration of the factor K of (8) and (9), it seems reasonable to expect that the relative values of $\overline{p}_{4,5}$, $\overline{p}_o$, and $\overline{p}_1$ are indicated qualitatively by the surface pressures in figure 11. Figures 5 to 7 show that K changes progressively as the configuration ratio changes, indicated by increasing deviation of r_1 from the value $r_o \sin^2\theta$. From (8), K is proportional to $(\overline{p}_{4,5} - \overline{p}_o)r_o - (\overline{p}_{4,5} - \overline{p}_1)r_1$, and it appears from figure 11 that $\overline{p}_{4,5}$ can be larger than $\overline{p}_o$ when the configuration ratio is large. Since $\overline{p}_{4,5} - \overline{p}_1$ is always positive, the factor K may be negligible under these conditions, as is indicated by figure 5. As the configuration ratio decreases, $\overline{p}_{4,5} - \overline{p}_o$ approaches zero and then becomes negative, so that K would become increasingly negative, as is indicated by figures 6 and 7.

A final point is that K is inversely proportional also to the square of the tangential velocity component, v_o^2. This was not taken into account in figures 5-7 since v_o was not measured, and this neglect may explain some of the scatter in the data.

4.3 The Vortex Core

On numerous occasions, a significant bulge or enlargement has been observed on tornado funnels, usually in the nascent or dissipation stage. Figure 13 is a series of drawings by Carl Reber who reported one such observation (1954). The enlargement can move up or down the funnel or remain stationary, probably indicating an association with a pattern of motion in the core rather than a local difference in rotation.

The core, defined as the inner portion of a Rankine combined vortex where the angular momentum increases rapidly with radius, is a zone of great dynamic stability, (Eliassen and Kleinschmidt, 1945).

It is important, however, to consider the secondary effects that are observed in the axial, or vertical direction. Assume a

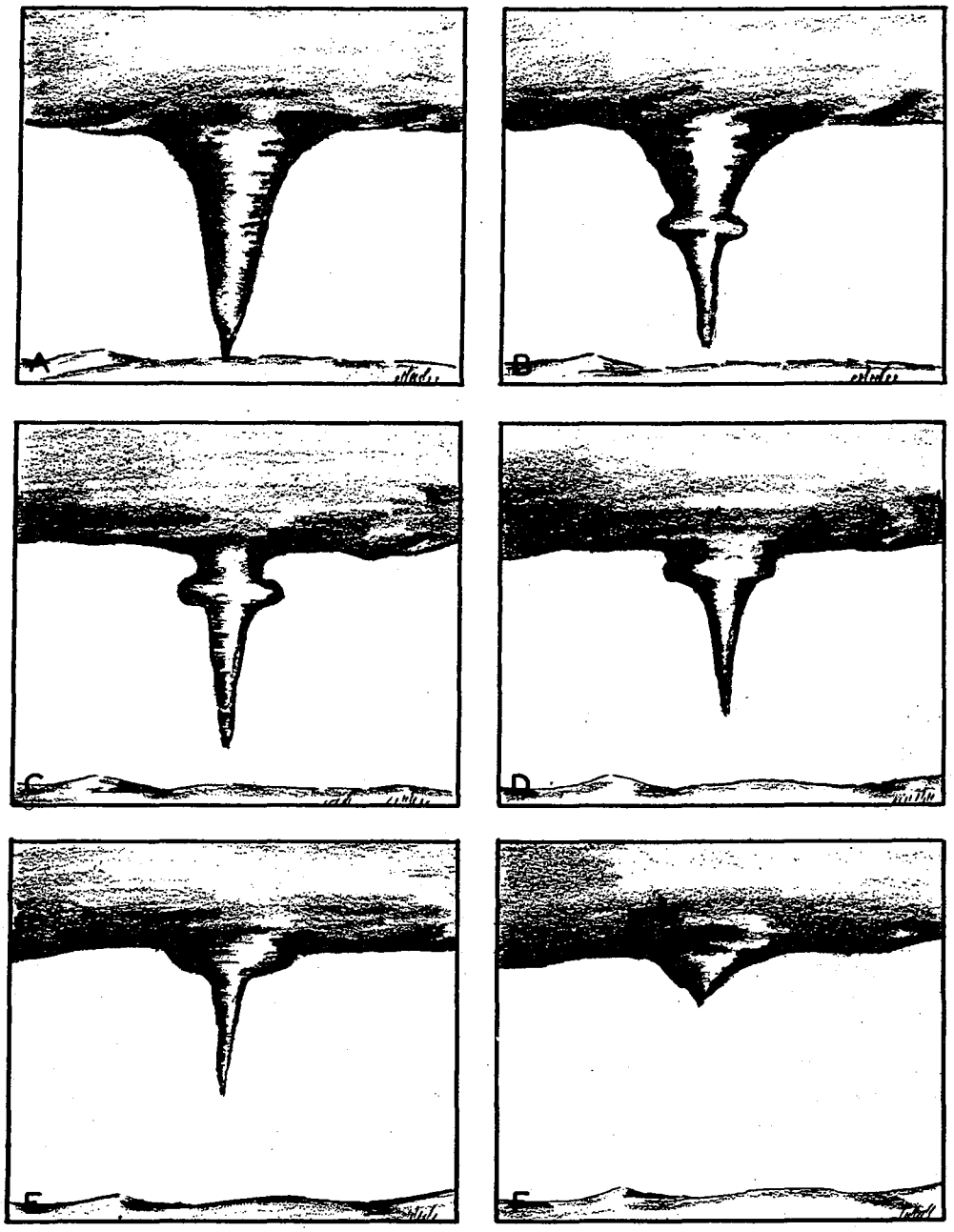

Figure 13. Drawings of observed enlargement of vortex core, by Carl Reber.

vortex column as in figure 14 with uniform vorticity. If a slice of the column ABCD is somehow deformed into A'B'C'D', the affected parcels, conserving their angular momenta, will rotate faster, causing a lowering of the central pressure within the slice. This results in fluid acceleration into A'B'C'D' from the adjacent slices, forcing its return toward ABCD. By a similar argument it can be shown that an enlargement along the vortex cylinder must be transitory also. Local excursions of fluid along the axis are frequently observed in vortex cores in the atmosphere and in the laboratory, and they are apparently due to perturbations in the flow field. Otherwise the core is very stable and nearly cylindrical in shape, except at its base where it is modified by friction in the surface boundary layer.

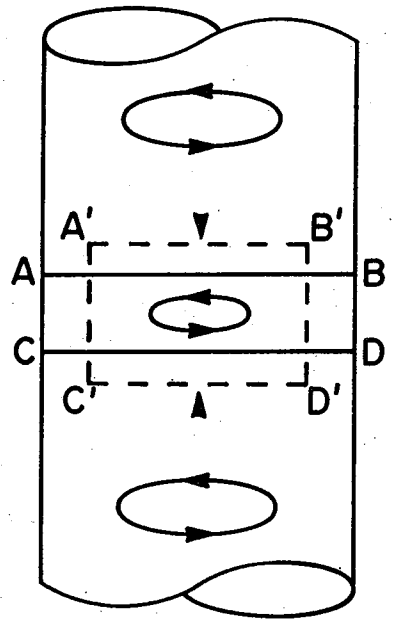

Figure 14. Rotational stability in a column.

Since the pressure fields in the laboratory vortices are produced and maintained without buoyancy, the following comments appear to be important.

Consider a horizontally converging surface layer. When rotation around the vertical axis is introduced, centrifugal forces develop which oppose the horizontal convergence and associated vertical stretching. If the tangential component is small at the perimeter of the convergence, centrifugal opposition may be negligible in the outer portion of the updraft zone, but as the axis is approached, centrifugal force increases very rapidly, inversely as the 3rd power of the radius. The core radius, r_1, where the centrifugal force per unit mass balances the pressure gradient, is a convergence boundary, so there can be no vertical stretching of the core fluid. Surface friction tends to reduce the centrifugal resistance at the base of the core so that a more penetrating convergence in a shallow surface layer provides a limited mass flow for net upward movement within the core. The fluid in the updraft zone surrounding the core has a higher upward speed and exerts an upward drag force on the slower moving core fluid. Considering this relative speed and relating the pressure deficit at the base of the vortex to the pressure loss due to frictional flow in pipes, one could expect the pressure deficit at the base

to be related to L/d, where L is the length of vortex core (or pipe length) and d is the diameter. It appears that the pressure deficit at the base of a vortex core of sufficient length but of small diameter is maintained by these friction effects without local buoyancy or "hydrostatic balance." This is surely true in the laboratory vortex.

A vortex core with inherent lateral stability and laminar flow in the lower portion can be produced in the laboratory. The upper portion, on the other hand, is always turbulent and contains a central downdraft, since the top of the vortex is exposed through the honeycomb barrier to non-rotating flow which cannot sustain a local pressure deficit. In the atmosphere, one would expect a lack of rotation at the top of the updraft within which the vortex is imbedded, and, similarly, a downdraft.

The transition from laminar to turbulent flow resembles a step change and is sometimes called "vortex breakdown." Figure 15 shows a laboratory example. With constant convergence, an increase in circulation lowers the turbulent zone and, at the same time, increases the core diameter. The upward speed of the fluid outside the core may increase, but inside, the upward speed decreases and a net increase of relative speed develops. It is of interest that these changes increase the Reynolds number for the core and suggest that a critical Reynolds number is associated with the change from laminar to turbulent flow.

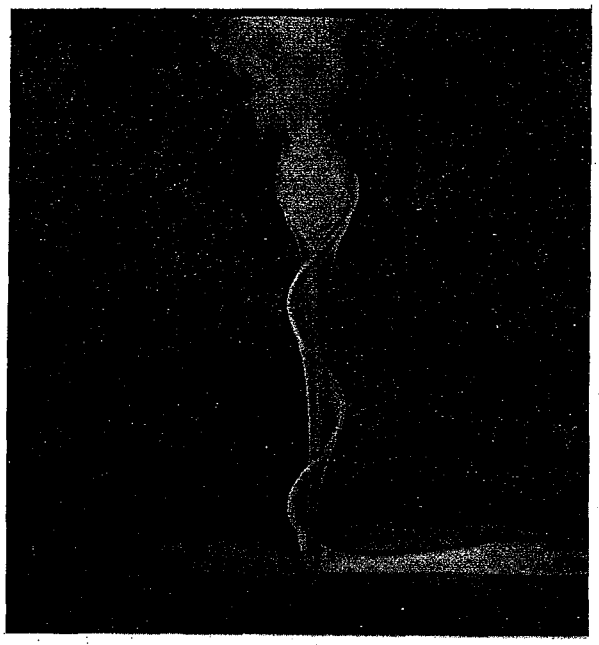

Figure 15. Laboratory vortex enlargement associated with transition from laminar to turbulent flow.

In figure 16, the upward drag on the outer portion of the turbulent section of the core is greater than on the laminar section, and the resultant vertical stretching in the outer core fluid requires vertical convergence along the axis into the transition section. In the laboratory, the central flow in the turbulent core is characteristically downward and part of

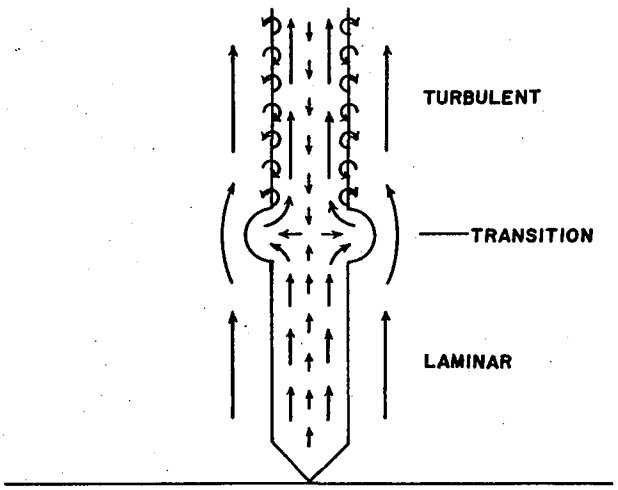

Figure 16. Flow schematic of vortex transition.

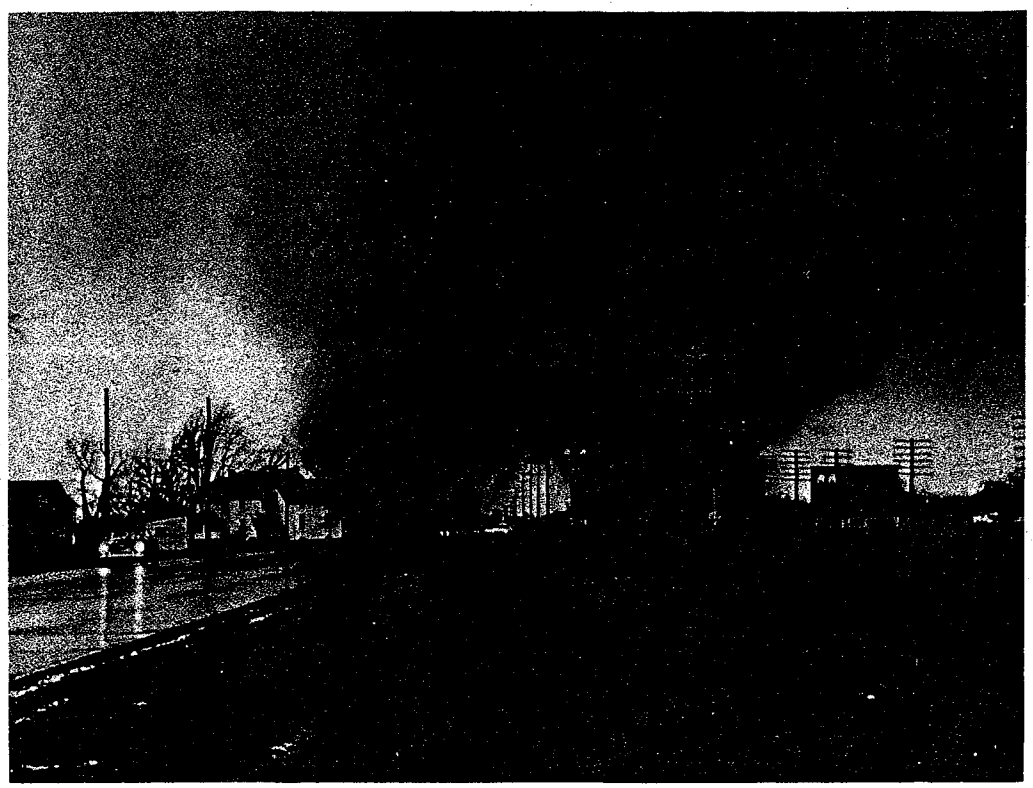

Figure 17. Tornado pair, Elkhart, Indiana, Palm Sunday, 1965. (Photograph by Paul Huffman).

a secondary circulation resembling the downward motion at the center of dust devils described by Scorer (1958). Regardless of whether a reversal of direction occurs along the axis at the level of transition from laminar to turbulent flow, the localized accumulation of fluid results in a pronounced lateral bulge.

4.4 Multiple Vortices

On numerous occasions, more than one tornado has been observed simultaneously, separated by only a short distance. Hurricanes also occasionally are observed to have two "eyes," or separate central cores. Figure 17 is a photograph of a pair of tornadoes which occurred at Elkhart, Indiana, on Palm Sunday, 1965. In the Newton, Kansas, tornado cyclone of May 24, 1962, which had a calm eye one to two miles in diameter, the following was reported: "Funnels were appearing all around town at different locations, moving in various directions." Figure 18 shows a laboratory demonstration of two vortices in the same convergence area, and figure 19 shows a family of three. The cores here are not uniquely

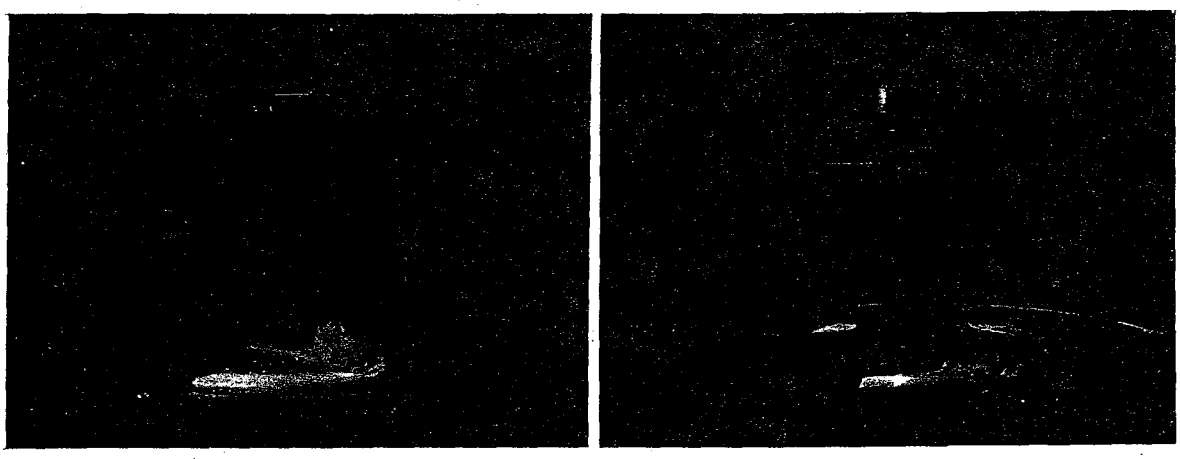

Figure 18. Laboratory vortex pair. Figure 19. Laboratory vortex family of three.

defined by the smoke tracer as in a single vortex, since any stationary tracer source on the lower surface will diffuse throughout the turbulent primary vortex core. Only an increase in tracer density can be obtained by present methods, and the distribution of the tracer is almost never uniformly distributed in the multiples. However, actual observation and movie film show the multiple vortices to be well defined.

In the laboratory, more than one vortex can be produced only when the configuration ratio is greater than unity. When the ratio is 4, and the angle of inflow θ is very small, 2° to 3°, a single vortex forms; as θ is increased, the diameter of the core increases proportionately. The scale of the turbulence also increases with the inflow angle and when the latter reaches about 30°, a vortex pair develops. They are located on opposite sides of the parent vortex near the radius of the maximum tangential speed and the pair rotates around the central axis at about half that speed. Once the pair is formed, the flow becomes somewhat more stable and the cores are well defined. This mode will continue when the inflow angle is decreased several degrees below that required for pair formation.

After a pair is formed, a third vortex will form, and then a fourth, as the inflow angle is further increased. In general, the greater the number of vortices in the system, the smaller their individual core diameters.

The critical inflow angle, θ_c, at which multiple vortices form is very sensitive to the geometry of the convection. A vortex pair forms at an inflow angle of about 30° when the configuration ratio is 4; when that ratio approaches unity, the angle required for pair formation increases to about 75°. When the depth of the convergence layer exceeds the diameter of the convection, no multiple vortices have been observed.

Smoke tracers show downward motion along the axis of a system containing multiple vortices, and outward radial motion near the lower surface, as illustrated in figure 20. The converging air from the outside enters the

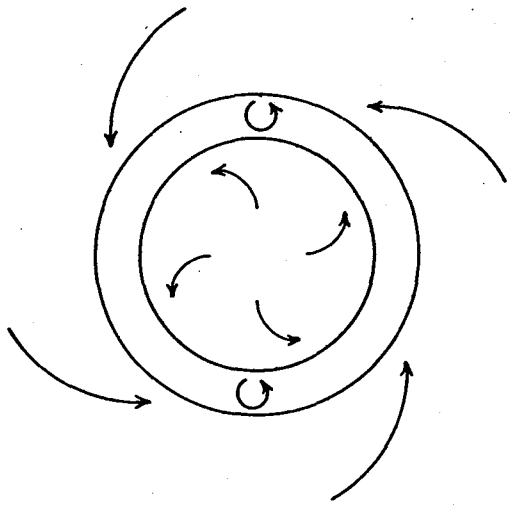

Figure 20. Observed surface flow for laboratory vortex pair.

annular area with a strong tangential speed while that of the diverging central portion is much less. Thus the annulus at low levels is characterized by strong horizontal convergence, horizontal shear and vertical stretching, all favorable for vortex formation.

As described earlier in section 4.3, the upper end of a vortex degenerates in a non-rotating atmosphere, and the pressure deficit which can be maintained at the base of the core is related to L/d, the ratio of its length to its diameter, $d = 2r_1$. As d is increased and L is kept constant, non-rotating air can make its way downward through the core more and more freely and act to dissipate the pressure deficit. In the experimental apparatus, when d approaches a critically large value, a single vortex becomes unstable, with accompanying large scale turbulence and large fluctuations in core diameter. It appears that this instability is the result of the presence of inward directed forces associated with radial momentum flux sufficient to produce a vortex core whose central pressure deficit requirement is greater than can be maintained in the presence of subsidence in the large core. In this condition of instability, when one or more vortices of smaller horizontal scale form in the annulus of figure 20, they tend to be stable, since their smaller cores can maintain a greater pressure deficit.

It is suggested that multiple, or secondary, vortices in the atmosphere may be similar to these and result in "suction spots" in some tornadoes, as described by Fujita (1967), figure 21. Measurements in the laboratory along the lower surface show the secondary vortices to be accompanied by extremes of low pressure, much lower than in the central area of the primary vortex.

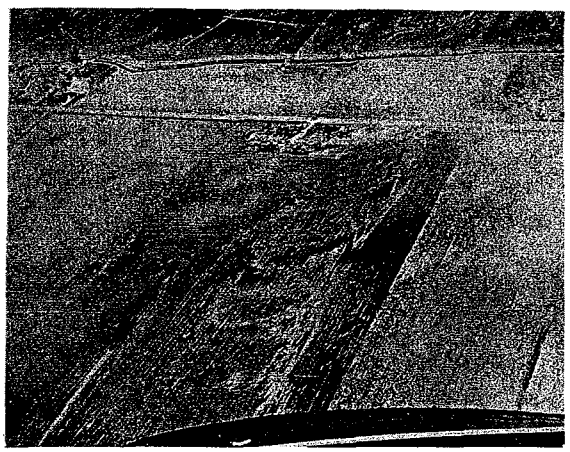

Figure 21. Tornado path with suction spots (from Fujita, 1967).

5. CONCLUSIONS

There is no evidence that a sink of limited area and of sufficient intensity to produce a tornado occurs naturally in the free atmosphere. Once a tornado is formed, however, there are several known factors which favor its maintenance. An extreme radial pressure gradient exists to account for centripetal acceleration. Localized heat of condensation in the funnel cloud

and in the upper area of reduced pressure, acting under the influence of rotational stability, contributes to the radial pressure gradient by the "hydrostatic" effect. Also, as the vortex increases in scale, subsiding motion along the central axis may provide air of significantly higher potential temperature. But none of these factors exists before the vortex is formed.

Laboratory results substantiate the point of view that for vortex formation, there must be a large influx of radial momentum which can produce a force field such that a portion of the fluid mass is required to converge against opposing centrifugal force plus any net outward pressure thrust. One condition which should be favorable for the buildup of a large radial momentum flux is the chimney effect resulting from the dynamic stability of a rotating convective column on a thunderstorm scale (Ward, 1967).

There is evidence that small but intense, short-lived tornadoes frequently occur at some distance from active convection areas of thunderstorms. These may occur, not because of local buoyancy-produced convection, but as the result of the momentum of a strong, convergent local wind field, such as at the leading edge of a strong thunderstorm outflow, where such tornadoes are frequently observed. When there are several storms over an area, the convergent field may be due to colliding outflows. If the flux of horizontal momentum is sufficient, there can be intense vortex motion, even though the required vertical motion may be due to mechanical forcing of even negatively-buoyant air.

It is hoped that this study will encourage research into the factors affecting the geometry of atmospheric convection and the intensity of inflow as they are related to atmospheric vortex motion, and that future measurements of velocity and pressure distributions can be made with the existing laboratory vortex system in order to further explore the significance of the r_o/h ratio.

6. ACKNOWLEDGMENTS

Special acknowledgment is given Dr. G. D. Kinzer for his significant contribution to this paper, especially in the application of the momentum theorem.

7. REFERENCES

Eliassen, A. and E. Kleinschmidt, 1957: Encyclopedia of Physics, Ed. S. Flugge, Vol 48, Berlin, Springer-Verlag, 64-66.

Fujita, T. T., 1967: Estimated wind speed of the Palm Sunday tornadoes, SMRP Research Paper No. 53, 9-13.

Kuo, H. L. 1969: Axisymmetric flows in the boundary layer of a maintained vortex, University of Chicago, Planetary circulation project report no. 15, 54.

Milne-Thomson, L. M., 1960: Theoretical Hydrodynamics, New York, The Macmillan Co., 77.

Reber, C. M., 1954: The South Platte Valley tornadoes of June 7, 1953, Amer. Meteor. Soc. Bul., 35, 191-197.

Scorer, R. S., 1958: Natural Aerodynamics, London, Pergamon Press, 180.

Ward, N. B., 1964: The Newton, Kansas, tornado cyclone of May 24, 1962, Amer. Meteor. Soc., Proceedings, Eleventh Weather Radar Conf., 410-415.

_____ , 1967: An effect of rotation on a buoyant convective column, Amer. Meteor. Soc., Proceedings, Fifth Conf. on Severe Local Storms, 368-373.

Ying, S. J. and Chang, C. C., 1970: Exploratory model study of tornado-like vortex dynamics, J. Atmos. Sci., 27, 3-14.

NATIONAL SEVERE STORMS LABORATORY

The NSSL Technical Memoranda, beginning with No. 28, continue the sequence established by the U. S. Weather Bureau National Severe Storms Project, Kansas City, Missouri. Numbers 1-22 were designated NSSP Reports. Numbers 23-27 were NSSL Reports, and 24-27 appeared as subseries of Weather Bureau Technical Notes. These reports are available from the Clearinghouse for Federal Scientific and Technical Information, 5285 Port Royal Road, Springfield, Virginia 22151, for $3.00, and a microfiche version for $0.65. CFTSI numbers are given below in parentheses.

No. 1 National Severe Storms Project Objectives and Basic Design. Staff, NSSP. March 1961. (PB-168207)

No. 2 The Development of Aircraft Investigations of Squall Lines from 1956-1960. B. B. Goddard. (PB-168208)

No. 3 Instability Lines and Their Environments as Shown by Aircraft Soundings and Quasi-Horizontal Traverses. D. T. Williams. February 1962. (PB-168209)

No. 4 On the Mechanics of the Tornado. J. R. Fulks. February 1962. (PB-168210)

No. 5 A Summary of Field Operations and Data Collection by the National Severe Storms Project in Spring 1961. J. T. Lee. March 1962. (PB-165095)

No. 6 Index to the NSSP Surface Network. T. Fujita. April 1962. (PB-168212)

No. 7 The Vertical Structure of Three Dry Lines as Revealed by Aircraft Traverses. E. L. McGuire. April 1962. (PB-168213)

No. 8 Radar Observations of a Tornado Thunderstorm in Vertical Section. Ralph J. Donaldson, Jr. April 1962. (PB-174859)

No. 9 Dynamics of Severe Convective Storms. Chester W. Newton. July 1962. (PB-163319)

No. 10 Some Measured Characteristics of Severe Storms Turbulence. Roy Steiner and Richard H. Rhyne. July 1962. (N62-16401)

No. 11 A Study of the Kinematic Properties of Certain Small-Scale Systems. D. T. Williams. October 1962. (PB-168216)

No. 12 Analysis of the Severe Weather Factor in Automatic Control of Air Route Traffic. W. Boynton Beckwith. December 1962. (PB-168217)

No. 13 500-Kc./Sec. Sferics Studies in Severe Storms. Douglas A. Kohl and John E. Miller. April 1963. (PB-168218)

No. 14 Field Operations of the National Severe Storms Project in Spring 1962. L. D. Sanders. May 1963. (PB-168219)

No. 15 Penetrations of Thunderstorms by an Aircraft Flying at Supersonic Speeds. G. P. Roys. Radar Photographs and Gust Loads in Three Storms of 1961 Rough Rider. Paul W. J. Schumacher. May 1963. (PB-168220)

No. 16 Analysis of Selected Aircraft Data from NSSP Operations, 1962. T. Fujita. May 1963. (PB-168221)

No. 17 Analysis of Methods for Small-Scale Surface Network Data. D. T. Williams. August 1963. (PB-168222)

No. 18 The Thunderstorm Wake of May 4, 1961. D. T. Williams. August 1963. (PB-168223)

No. 19 Measurements by Aircraft of Condensed Water in Great Plains Thunderstorms. George P. Roys and Edwin Kessler. July 1966. (PB-173048)

No. 20 Field Operations of the National Severe Storms Project in Spring 1963. J. T. Lee, L. D. Sanders and D. T. Williams. January 1964. (PB-168224)

No. 21 On the Motion and Predictability of Convective Systems as Related to the Upper Winds in a Case of Small Turning of Wind with Height. James C. Fankhauser. January 1964. (PB168225)

No. 22 Movement and Development Patterns of Convective Storms and Forecasting the Probability of Storm Passage at a Given Location. Chester W. Newton and James C. Fankhauser. January 1964. (PB-168226)

No. 23 Purposes and Programs of the National Severe Storms Laboratory, Norman, Oklahoma. Edwin Kessler. December 1964. (PB-166675)

No. 24 Papers on Weather Radar, Atmospheric Turbulence, Sferics, and Data Processing. August 1965. (AD-621586)

No. 25 A Comparison of Kinematically Computed Precipitation with Observed Convective Rainfall. James C. Fankhauser. September 1965. (PB-168445).

No. 26 Probing Air Motion by Doppler Analysis of Radar Clear Air Returns. Roger M. Lhermitte. May 1966. (PB-170636)

No. 27 Statistical Properties of Radar Echo Patterns and the Radar Echo Process. Larry Armijo. May 1966. The Role of the Kutta-Joukowski Force in Cloud Systems with Circulation. J. L. Goldman. May 1966. (PB-170756)

No. 28 Movement and Predictablity of Radar Echoes. James Warren Wilson. November 1966. (PB-173972)

No. 29 Notes on Thunderstorm Motions, Heights, and Circulations. T. W. Harrold, W. T. Roach, and Kenneth E. Wilk. November 1966. (AD-644899)

No. 30 Turbulence in Clear Air Near Thunderstorms. Anne Burns, Terence W. Harrold, Jack Burnham, and Clifford S. Spavins. December 1966. (PB-173992)

No. 31 Study of a Left-Moving Thunderstorm of 23 April 1964. George R. Hammond. April 1967. (PB-174681)

No. 32 Thunderstorm Circulations and Turbulence from Aircraft and Radar Data. James C. Fankhauser and J. T. Lee. April 1967. (PB-174860)

No. 33 On the Continuity of Water Substance. Edwin Kessler. April 1967. (PB-175840)

No. 34 Note on the Probing Balloon Motion by Doppler Radar. Roger M. Lhermitte. July 1967. (PB-175930)

No. 35 A Theory for the Determination of Wind and Precipitation Velocities with Doppler Radars. Larry Armijo. August 1967. (PB-176376)

No. 36 A Preliminary Evaluation of the F-100 Rough Rider Turbulence Measurement System. U. O. Lappe. October 1967. (PB-177037)

No. 37 Preliminary Quantitative Analysis of Airborne Weather Radar. Lester P. Merritt. December 1967. (PB-177188)

No. 38 On the Source of Thunderstorm Rotation. Stanley L. Barnes. March 1968. (PB-178990)

No. 39 Thunderstorm - Environment Interactions Revealed by Chaff Trajectories in the Mid-Troposphere. James C. Fankhauser. June 1968. (PB-179659)

No. 40 Objective Detection and Correction of Errors in Radiosonde Data. Rex L. Inman. June 1968. (PB-180284)

No. 41 Structure and Movement of the Severe Thunderstorms of 3 April 1964 as Revealed from Radar and Surface Mesonetwork Data Analysis. Jess Charba and Yoshikazu Sasaki. October 1968. (PB-183310)

No. 42 A Rainfall Rate Sensor. Brian E. Morgan. November 1968. (PB-183979)

No. 43 Detection and Presentation of Severe Thunderstorms by Airborne and Ground-Based Radars: A Comparative Study. Kenneth E. Wilk, John K. Carter, and J. T. Dooley. February 1969. (PB-183572)

No. 44 A Study of a Severe Local Storm of 16 April 1967. George Thomas Haglund. May 1969. (PB-184-970)

No. 45 On the Relationship Between Horizontal Moisture Convergence and Convective Cloud Formation. Horace R. Hudson. March 1970. (PB-191720)

No. 46 Severe Thunderstorm Radar Echo Motion and Related Weather Events Hazardous to Aviation Operations. Peter A. Barclay and Kenneth E. Wilk. June 1970. (PB-192498)

No. 47 Evaluation of Roughness Lengths at the NSSL-WKY Meteorological Tower. Leslie D. Sanders and Allen H. Weber. August 1970. (PB-194587)

No. 48 Behavior of Winds in the Lowest 1500 ft in Central Oklahoma: June 1966 - May 1967. Kenneth C. Crawford and Horace R. Hudson. August 1970.

No. 49 Tornado Incidence Maps. Arnold Court. August 1970.

No. 50 The Meteorologically Instrumented WKY-TV Tower Facility. John K. Carter. September 1970

No. 51 Papers on Operational Objective Analysis Schemes at the National Severe Storms Forecast Center. Rex L. Inman. November 1970.

GPO 832-488